DIRECTIONAL CHARACTERISTICS OF INFRARED EMISSION FROM THE MOON

D. F. WINTER* and J. A. KRUPP
Boeing Scientific Research Laboratories, Seattle, Wash., U.S.A.

(Received 3 August, 1970)

Abstract. Infrared surveys of the illuminated Moon have shown that the lunar surface does not radiate like a Lambert emitter. A detailed description is presented of directional emission from the equatorial region of the Moon, based on brightness temperature measurements by Saari and Shorthill (1967a, b). In general, the measurements indicate that the illuminated lunar surface is anomalously warm (cool) when the Sun is behind (in front of) the observer. It is plausible to attribute such directional effects to negative surface relief. A thermal model of a cratered lunar soil is developed to examine these effects both qualitatively and quantitatively. The results of the study indicate that centimeter- and meter-scale craters, with a variety of forms, both sharp and subdued, can account for measured directional emission characteristics over a wide range of Sun and observer angles.

Most theoretical studies of heat exchange in the lunar soil assume the surface of the Moon to be a locally smooth, Lambertian emitter at far infrared wavelengths. With this idealization, the apparent brightness temperature T_L of the surface, when illuminated by the Sun at elevation angle χ, is approximately

$$T_L = T_s \sin^{1/4} \chi, \tag{1}$$

where T_s is the surface temperature at the subsolar point. If the emissivity of the lunar soil is assumed equal to unity, then T_s can be estimated from

$$T_s = [A_0 (1 - \alpha)/\sigma]^{1/4}, \tag{2}$$

where A_0 is the solar constant (0.1362 W cm^{-2}), α is an average effective albedo (0.08 for mare), and σ is the Stefan-Boltzmann constant. Substitution of these parameter values into Equation (2) gives $T_s = 385.5$ K.

The temperature T_L in Equation (1) is usually referred to as the Lambert temperature of the surface. The Lambert temperature is a good approximation to the actual surface temperature when thermal gradients immediately below the surface are relatively small; i.e., when χ is not too close to grazing incidence. However, systematic discrepancies are observed between measured brightness temperatures and calculated temperatures based on smooth-surface soil models. Quantitative descriptions of these discrepancies are made possible by infrared surveys of the illuminated Moon. Such surveys have been performed by workers at Lowell Observatory (Geoffrion *et al.*, 1960; Sinton, 1962) and at The Boeing Company (Montgomery *et al.*, 1966; Saari and Shorthill, 1967a). These observational studies have made available a fairly complete description of directional emission characteristics in the equatorial region of the Moon.

Not surprisingly, the measurements show that brightness temperatures T_b depend

* Present address: Department of Oceanography, University of Washington, Seattle, Washington, U.S.A.

The Moon **2** (1971) 279–292.

in a complicated way upon the elevation and azimuth angles of the observer as well as the elevation and azimuth of the Sun. For example, Figure 1 shows a collection of observed brightness temperatures associated with regions along the thermal meridian,* as measured by Saari and Shorthill. The temperatures are displayed as functions of observer angle ζ for six different solar elevation angles. The angle ζ is measured from

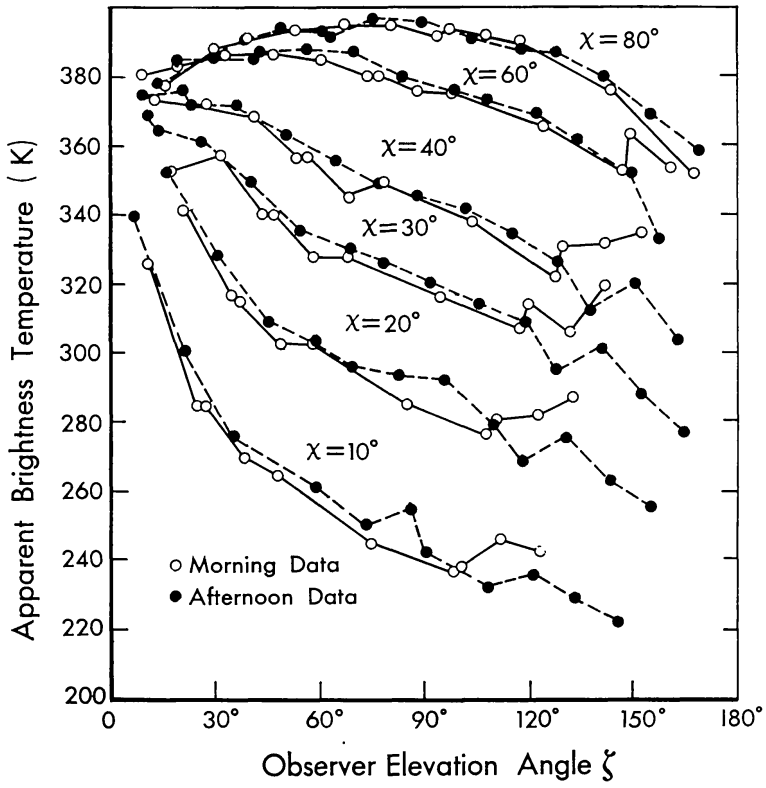

Fig. 1. Thermal meridian brightness temperatures as measured by Saari and Shorthill (1967a).

90–180° when the lines joining a surface element with the Sun and the observer are on opposite sides of the normal to the element (see Figure 2). Under these definitions, the coordinates (ζ, χ) can refer to two different regions on the thermal meridian, one being to the east of disk center, the other to the west. Morning and afternoon temperatures are identified in Figure 1 by open and filled circles, respectively. As can be seen from the figure, morning and afternoon data are approximately coincident when the observer angle ζ is less than the sum $90° + \chi$, as a general rule. At greater values of ζ, it is more difficult to define an average brightness temperature in a meaningful way.

There is some advantage to be gained from using the ratio T_b/T_L to describe directional emission characteristics. For example, Saari and Shorthill re-expressed their thermal meridian measurements in terms of ratios T_b/T_L (which they referred to as D-factors). When the D-factors were plotted as functions of ζ for constant values of χ, the averaging of the measurements was facilitated since the scatter in the data was reduced. This feature is illustrated in Figure 3, where data from Figure 1 corresponding

* The thermal meridian is defined as the great circle through the disk center and the subsolar point.

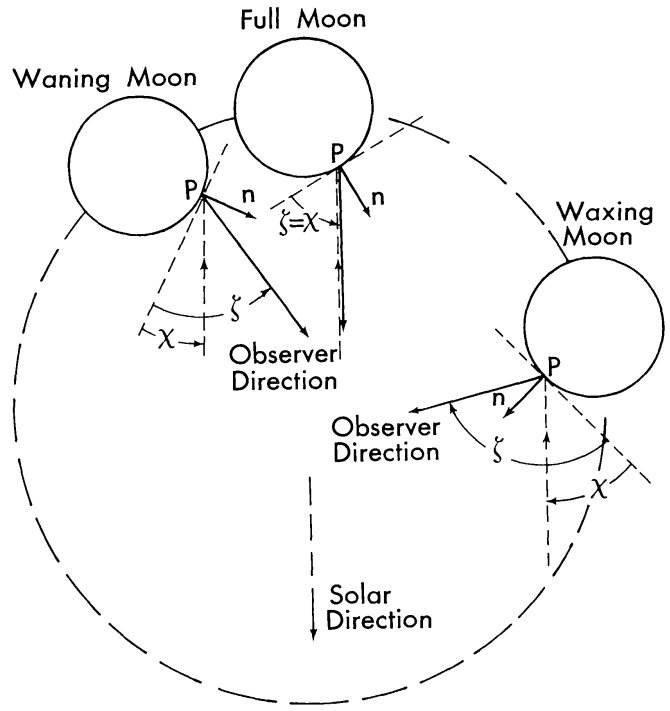

Fig. 2. Geometry of sun and observer elevation angles for a region on the thermal meridian.

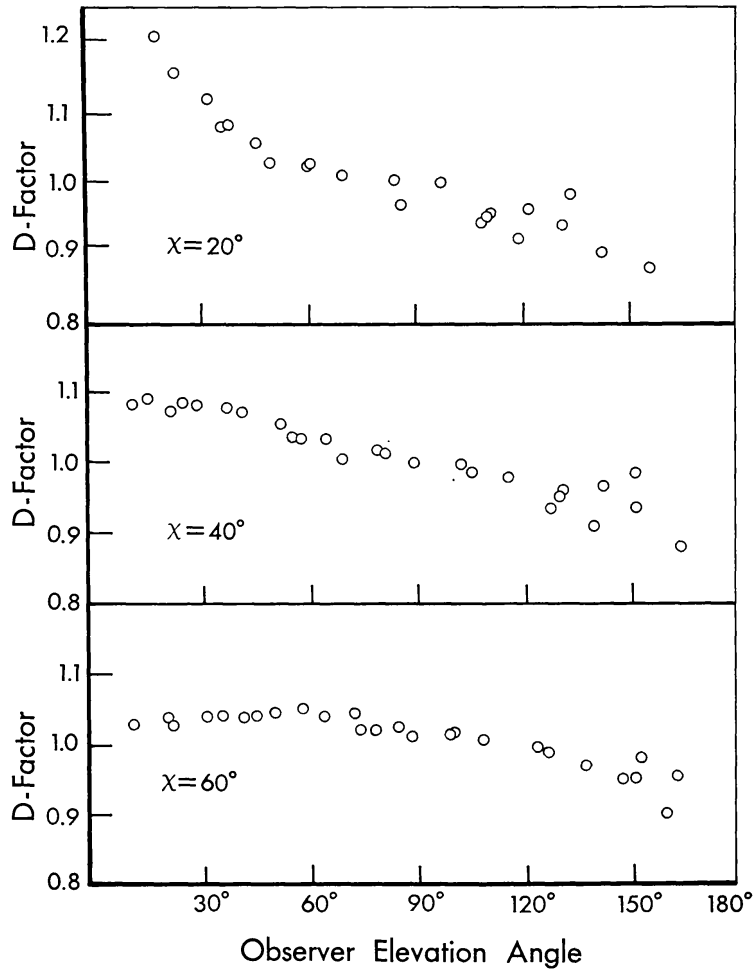

Fig. 3. Infrared data exhibited as *D*-factors for three sun elevation angles.

to $\chi = 20°$, 40°, and 60° are replotted as D-factors. All the important features of directional emission characteristics are displayed by the general pattern of D-factor contours in a $\zeta - \chi$ plane. The contours shown in Figure 4 were constructed from albedo-corrected, averaged thermal meridian data of Saari and Shorthill over the range of sun angles $10° < \chi < 80°$. In the figure, contours are omitted from the peripheral regions $\zeta < 10°$ and $\zeta > 150°$ due to large uncertainties in the data in those regions. The contour corresponding to $T_b/T_L = 1.03$ is shown as a dashed line for $\chi > 70°$ because there are insufficient data to specify the true pattern.

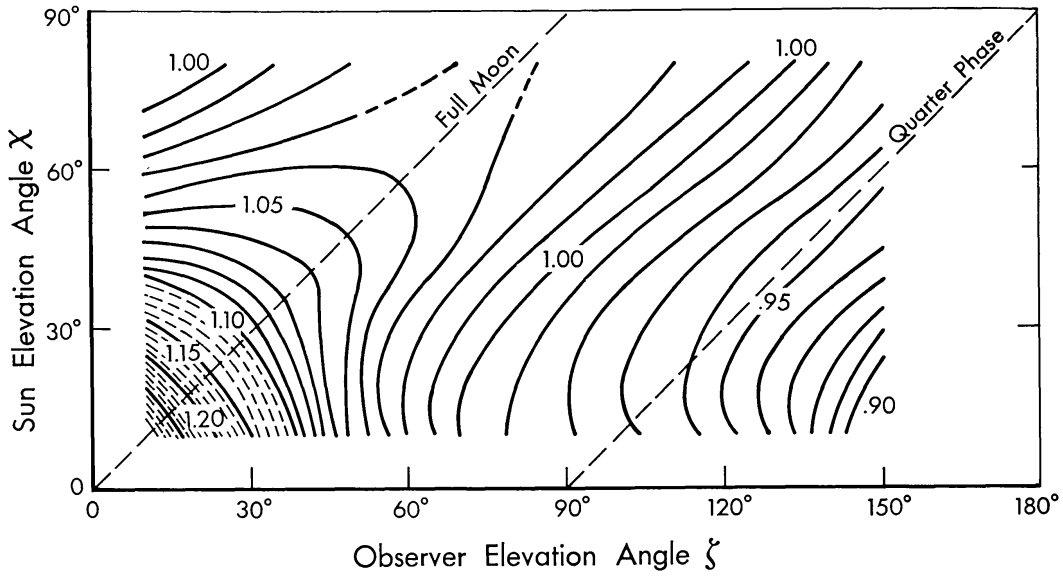

Fig. 4. Measured thermal meridian D-factor contours in the $\zeta - \chi$ plane.

Anomalous directionality of lunar emission in the *IR* was first described in detail over forty years ago by Pettit and Nicholson (1930), who offered a qualitative explanation of the effects in terms of positive surface relief features. However, studies of the thermal behavior of lunar rocks (Roelof, 1968; Winter, 1970) indicate that typical marial distributions of solid surficial debris will produce only minor changes in apparent brightness for sun and observer elevation angles near the zenith. In fact, if rocks were the only extant surface feature, then the D-factors associated with the disk center near the time of full-moon ($\zeta \sim \chi \sim 90°$) would be less than 1.00, contrary to observation, as is apparent from Figure 4.

Considerations such as those above have led to the speculation that negative relief, perhaps in the form of intermediate-scale craters (with diameters ranging from a few centimeters to several meters) is the more likely cause of directional effects at infrared wavelengths. The overall characteristics of brightness temperature variations and D-factor contour patterns are consistent with this idea. The temperatures of those regions of crater interiors which are more effectively insolated than the exterior will generally exceed the environ temperature corresponding to sun elevation angle χ. Shadowed regions, on the other hand, will tend to be cooler than the environs. Conse-

quently, one would expect the apparent brightness temperature T_b of an illuminated cratered surface, viewed in the plane containing the thermal meridian, to be greatest when the Sun is behind the observer. More specifically, if the apparent brightness temperature is considered as a function of increasing ζ, then, depending upon the crater form and the sun angle, T_b may undergo a slight initial increase from a value greater than T_L until it reaches a maximum at $\zeta = \zeta_{max} < 90°$, beyond which it declines to a value less than that of the environs. For a given crater configuration, one may also expect ζ_{max} to increase with sun elevation angle, since the warm regions of crater interiors will move from the rims toward the crater bottoms as the Sun moves toward the zenith. Consequently, as ζ increases, the detector must view the surface at a correspondingly higher elevation angle to observe the maximum brightness temperature. An inspection of Figures 1, 3, and 4 shows that the observed brightness temperature variations and D-factor patterns are consistent with these remarks.

Similar arguments apply to other forms of negative relief. In fact, Gear and Bastin (1962) pointed out several years ago that general intermediate-scale surface roughness might account for the phase variation of the subsolar point brightness. This suggestion has recently been re-examined quantitatively by Bastin and Gough (1969) who consider the problem of heat transfer in a soil with surface roughness idealized by parallel indentations of rectangular cross-section. The analysis was extended to study directional emission effects as a function of sun and observer angles, for both eclipse and lunation conditions. These workers concluded that most of the general features of lunar daytime directional emission can be explained by some form of intermediate-scale surface roughness.

In a similar vein, Buhl *et al.* (1968a, b) examined the radiation characteristics of a lunar soil containing craters whose surfaces are spherical sections. In the first of the cited works, it was assumed that the daytime temperature of a crater surface and its environs can be calculated by neglecting sub-surface heat conduction. Resulting brightness temperatures were compared with the full-moon data reported by Pettit and Nicholson (1930) and the subsolar point phase variation described by Sinton (1962). It was concluded that the measurements could best be accounted for by a 50% density of millimeter-scale craters with profiles somewhat deeper than hemispherical.

The objective of the study described here was to determine the extent to which a cratered surface model could explain the more comprehensive thermal meridian measurements described earlier. For this purpose, we adopted the crater geometry used by Buhl *et al.* Thus, crater interiors were idealized by spherical sections and their environs by planes. In addition to the geometric idealization, we introduced two other major simplifications, namely: (1) the lunar soil was characterized as a homogeneous continuum of uniform thermophysical properties, and (2) crater and environ daytime surface temperatures were calculated by neglecting lateral subsurface thermal exchange.

Before presenting the analysis and the quantitative results, we shall digress briefly to justify the foregoing assumptions and to set forth the limitations on their applicability.

The first simplication might be challenged on the grounds that neither the effective thermal conductivity k_{eff} nor the specific heat c of the lunar soil are constant over the range of temperatures which prevail in a partially insolated crater. Even with the simplified three-dimensional crater geometry, however, the analysis of subsurface thermal exchange is so complex that only linear thermophysical models are computationally feasible. Thus, it becomes necessary to specify those conditions under which linearity constitutes an acceptable approximation. In this connection, it is instructive to consider thermal calculations in which the effect of surface relief has been neglected. For example, a comparison of a linear continuum model with a more sophisticated particulate soil model (Winter and Saari, 1969) shows that the former gives acceptable first approximations to surface temperatures when the thermal parameter $\gamma = (k_{\text{eff}}\varrho c)^{-1/2}$ is set equal to $820\,\text{cm}^2\,\text{K}\,\text{sec}^{1/2}\,\text{cal}^{-1}$ for a lunation, and is increased to 1350 during an eclipse. Thus, if the lunar soil mass density and specific heat are assigned average values of $\varrho = 1.4\,\text{g}\,\text{cm}^{-3}$ and $c = 0.64$ joules $\text{g}^{-1}\,\text{K}^{-1}$, respectively, then the effective 'lunation' thermal conductivity k_{eff} is $2.9 \times 10^{-5}\,\text{W}\,\text{cm}^{-1}\,\text{K}^{-1}$. During an eclipse, the apparent conductivity should be reduced to about 1.1×10^{-5}. On this basis, it is reasonable to expect that a linear model with appropriately chosen constant properties will constitute a satisfactory idealization for calculations of cratered soil surface temperatures. This will be particularly true during the lunar daytime when subsurface heat exchange has the least effect on surface temperatures.

The second simplification states that subsurface heat exchange takes place only along extensions of local surface normals, with crater and environ temperatures being calculated separately. It is true that in some circumstances subsurface heat flow will play an influential role in determining the surface temperature of a crater. The relative importance of this role can be judged by examining the relationships between the three relevant scales of length: the crater radius a, a thermal wavelength l_t, and a 'radiation length' l_r. A thermal wavelength l_t appropriate to a lunation can be calculated from $(k_{\text{eff}}/\varrho c\omega)^{1/2}$, where $\omega = 2.46 \times 10^{-6}\,\text{sec}^{-1}$ is the angular synodic frequency. The radiation length l_r is defined by $k_{\text{eff}}/\sigma T_0^3$, where T_0 is an appropriate representative temperature. From the physical point of view, the length l_r is the distance over which a temperature gradient is established in a semi-infinite medium by radiative cooling during the characteristic time interval $(\varrho c l_r^2/k_{\text{eff}})$.

When the thermal conductivity is assigned a value appropriate to a lunation, the length l_t is about 3.6 cm. It is not possible to assign a unique value to l_r since it depends critically upon the choice for T_0. In the case of a hemispherical crater, for example, when the Sun is well above the horizon, any of the interior which is still in shadow will be effectively irradiated by the relatively extensive insolated areas. Under these circumstances, the subsolar point temperature T_s can be considered an appropriate choice for T_0, and l_r turns out to be of the order of 0.1 cm. At the other extreme, during the lunar nighttime, crater surface and environs temperatures range from about 140 K near sunset to 90 K at sunrise. If T_0 is set equal to a 'representative' value of 120 K then l_r is about 3.1 cm and is evidently comparable with l_t. Prior to sunset and in the post-sunrise interval, an intermediate situation prevails where the fractional extent of

insolated areas is relatively small, and heating of shadowed regions by reradiation is only partially effective in maintaining crater surface temperatures. For example, when the temperature of a shadowed region is in the neighbourhood of 200 K, the radiation length l_r appropriate to that region is of the order of 1 cm.

With these observations in mind, we are in a position to draw some general conclusions concerning the relative importance of subsurface thermal exchange. Throughout the greater part of the lunar daytime (or during its entirety, in the first approximation), heat conduction into the soil plays a relatively minor role in determining surface temperatures of intermediate-scale craters. Near the beginning and the end of the lunar daytime, however, when l_r is comparable with l_t, subsurface conduction can contribute significantly to the thermal budget at the crater surface. Even during these times, however, lateral subsurface heat transport may be neglected in craters whose dimensions exceed a few centimeters. This follows from the fact that the ratio of πa to l_t measures the importance of lateral diffusion relative to radial heat flow.

The two principal simplifications introduced in this work, namely, the neglect of lateral conduction during the lunar daytime and the adoption of a thermal model with constant properties, make feasible the computation of surface temperatures of craters whose surfaces are spherical sections. Figure 5 illustrates several geometric parameters and the coordinate system which is used to describe the crater forms.

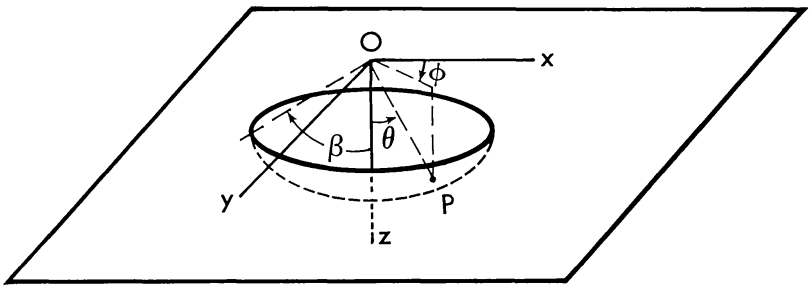

Fig. 5. Geometry of idealized crater interior and environs.

The equations which determine the thermal response of cratered soil are conveniently written in terms of nondimensional variables. In the expressions which follow, we measure all distances in units of l_t and all temperatures in units of T_s, as calculated from Equation (2). Nondimensional temperature will be denoted by $\psi = T/T_s$. The time variable t is replaced by the sun elevation angle χ which will be henceforth defined more generally as ωt. Finally, when k_{eff} and ϱ are constants, the thermal analysis is easily modified to include the temperature variation of specific heat. We allow for this variation by introducing a nondimensional specific heat $c^*(\psi)$ which can be obtained from a power series representation given by Winter and Saari (1969).

When a portion of the crater interior is in shadow, the boundary of the region is given by

$$\cos 2\chi \cos\theta - \cos\phi \sin 2\chi \sin\theta = \cos\beta\,, \tag{3}$$

where β is the polar angle subtended by the crater aperture, as illustrated in Figure 5.

Equation (3) is most conveniently treated as an explicit equation for ϕ in terms of θ and χ. With the definition of the shadow boundary by Equation (3), the intensity of insolation can be specified everywhere on the crater surface. Since the crater interior is a spherical section, the nondimensional insolation function at a point P with coordinates (θ, ϕ) can be expressed as

$$I(\theta, \phi, \chi) = \cos v, \quad \text{if} \quad P \text{ is illuminated}$$
$$= 0, \quad \text{otherwise}, \tag{4a}$$

with

$$\cos v = \sin\chi \cos\theta + \cos\phi \cos\chi \sin\theta . \tag{4b}$$

In this last expression, v is the angle between a ray to the Sun and the local surface normal at P.

With the neglect of lateral spatial derivations, the equation for the nondimensional temperature field in the soil below the crater surface takes the form

$$c^* \frac{\partial\psi}{\partial\chi} = \frac{\partial^2\psi}{\partial r^2} + \frac{2}{r}\frac{\partial\psi}{\partial r}, \tag{5a}$$

subject to

$$(l_r/l_t)\frac{\partial\psi}{\partial r} = \psi^4 - I(\theta, \phi, v) - \frac{1}{4\pi}\int_0^{2\pi}\int_0^{\beta} \psi^4(\theta', \phi') \sin\theta' \, d\theta' \, d\phi' \tag{5b}$$

at $r = a/l_t$. It is not difficult to show that if the crater radius exceeds l_t, the temperature near the surface will be adequately determined in the present approximation if Equation (5a) is simplified by neglecting the second term on the right side.

It is now apparent that if the term involving the ratio l_r/l_t is omitted from Equation (5b), then crater surface temperatures can be calculated approximately by neglecting conduction. This case has been treated by Buhl *et al.* (1968a) who show that Equation (5b) has a simple solution for ψ when the left side is set equal to zero. In terms of nondimensional variables, the temperature ψ on the interior surface can be expressed as

$$\psi(\theta, \phi, \chi) = [I(\theta, \phi, \chi) + c_1 \sin\chi]^{1/4}, \tag{6a}$$

where c_1 is a constant given by

$$c_1 = \tfrac{1}{2}(1 - \alpha)^{-1}(1 - \cos\beta), \tag{6b}$$

and $I(\theta, \phi, \chi)$ is the source function defined by Equation (4).

When Equations (6) are used to obtain crater temperatures, then to the same degree of accuracy, the environ temperatures can be identified with the Lambert temperature T_L. On the other hand, when conduction effects are included in the calculation of crater temperatures, it is appropriate to calculate environ temperatures $T_e(\chi)$ by solving the one-dimensional boundary value problem analogous to Equations (5).

Meridian temperatures calculated from Equations (6) for a hemispherical crater are

compared in Figure 6 with surface temperatures obtained from integration of Equations (5) for low sun angles $\chi = 10°$, 20°, and 30°. In each case, temperatures in the illuminated regions are in good agreement and the discrepancies in the shadowed regions decrease with increasing χ. Numerical comparisons, such as the one illustrated

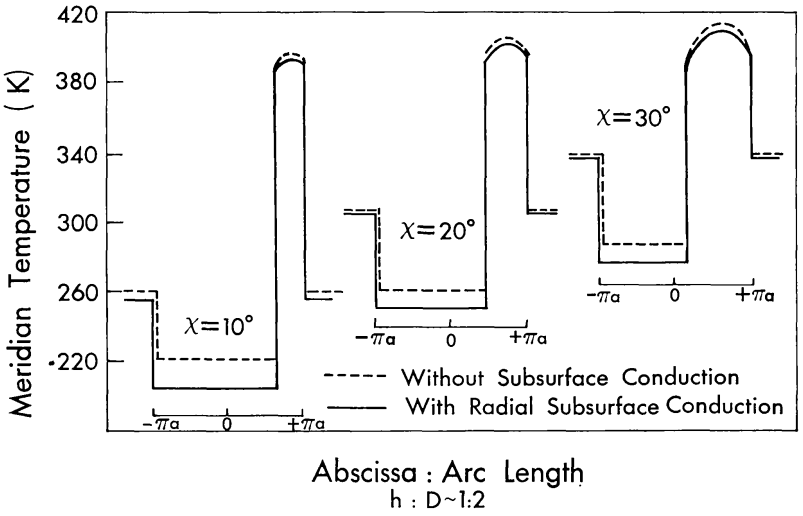

Fig. 6. Meridian surface temperature of a hemispherical crater, calculated with and without radial subsurface conduction.

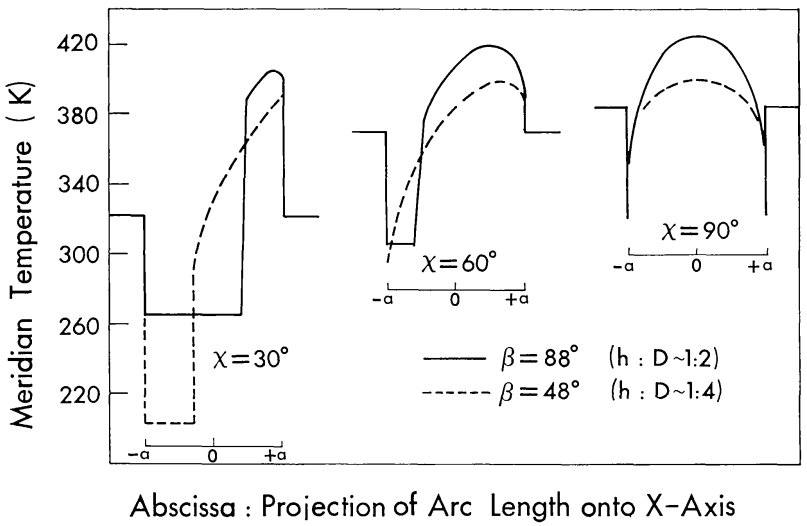

Fig. 7. Comparison of meridian surface temperatures of craters with sharp and subdued profiles.

in Figure 6, have established that when subsurface conduction is ignored entirely, errors in daytime surface temperatures generally do not exceed a few per cent, except at the lower sun angles. The effect of crater profile is illustrated in Figure 7 which compares meridian temperature profiles for a hemispherical crater with those for a shallower crater with a depth-to-diameter ratio h/d equal to $\frac{1}{4}$.

Once surface temperatures have been determined either from Equations (5) or (6), it is possible to establish the variation of apparent brightness temperature T_c as a func-

tion of observer angle ζ throughout the lunar daytime. Consider a narrow-band detector of characteristic temperature $T_\lambda = hc/\lambda k$ located at a great distance from a crater of aperture area $A_c = \pi a^2 \sin^2 \beta$. Assume that rays to the detector from points on the observable crater surface are approximately parallel and denote the angle between a local normal to the crater surface and a ray to the detector by v^*. The apparent crater temperature T_c as seen by the detector can be obtained from the relation

$$[\exp(T_\lambda/T_c) - 1]^{-1} = (1/\pi \sin\zeta \sin^2\beta) \iint_{\Gamma(\zeta)} [\exp(T_\lambda/T(\theta', \phi', \chi)) - 1]^{-1} \times \cos v^* \sin\theta' \, d\theta' \, d\phi' \tag{7}$$

where $\Gamma(\zeta)$ denotes the region of the interior surface which can be seen from elevation angle ζ.

The brightness temperature of the lunar soil, as measured by a distant detector, is determined both by emission from relatively smooth areas, which are approximately at temperature $T_e(\chi)$, and by emission from craters. The amount contributed by the latter depends upon the cumulative crater number density per unit surface area which, in turn, depends upon the statistical distributions of crater size and depth-to-diameter ratio.

Studies of intermediate-scale crater morphology based on spacecraft photography of marial regions indicate a continuum of crater forms ranging from sharply profiled to subdued, with the total population covering most of the surface (Morris and Shoemaker, 1968). Initial configurations of intermediate-scale craters are determined to a large extent by impact parameters and the local state and thickness of the regolith (Oberbeck and Quaide, 1967). Subsequent to formation, intermediate-scale crater profiles undergo progressive obliteration primarily as a result of impact erosion (Ross, 1968; Soderblom, 1970). Slumping of material on high angle slopes and sedimentation by ballistic debris from impacts elsewhere on the surface may also play a role in the degradation of crater profiles. In any case, the state of the regolith, as well as various erosion processes, are jointly responsible for the observed continuum of crater configurations. In marial regions, the cumulative size distribution of intermediate-scale craters is log-normal in character with an index of -2, (Trask, 1966). This distribution implies a predominance of small-sized craters and has been interpreted as an indication of a steady-state condition (Marcus, 1966; Soderblom, 1970). Furthermore, morphological studies based on Ranger photographs have indicated a tendency for smaller craters to exhibit more severe profiles than larger ones (Trask, 1967). The foregoing remarks imply that a significant fraction of the relevant negative surface relief may be associated with the smaller and somewhat sharper craters.

With these general observations in mind, we calculated crater brightness temperatures T_c from Equation (7) both for sharply contoured craters of hemispherical configuration and for shallower craters, characterized by a depth-to-diameter ratio of $\frac{1}{4}$. These results were then combined with calculations of environ temperature variations to obtain total apparent brightness temperatures $T_b(\zeta, \chi)$ of a cratered soil. Computa-

tions were performed for several different areal densities of subdued and sharply profiled craters. It was found that reasonably good correspondences with measurement could be achieved with a combination of both subdued and sharply profiled crater forms, in general accord with the morphological studies described above. Comparisons of observed data with theoretical brightness temperatures and D-factor contours are shown in Figures 8 and 9, respectively. The results in the figures correspond to a nominal case of equal areal fractions of environs, subdued, and sharp craters*.

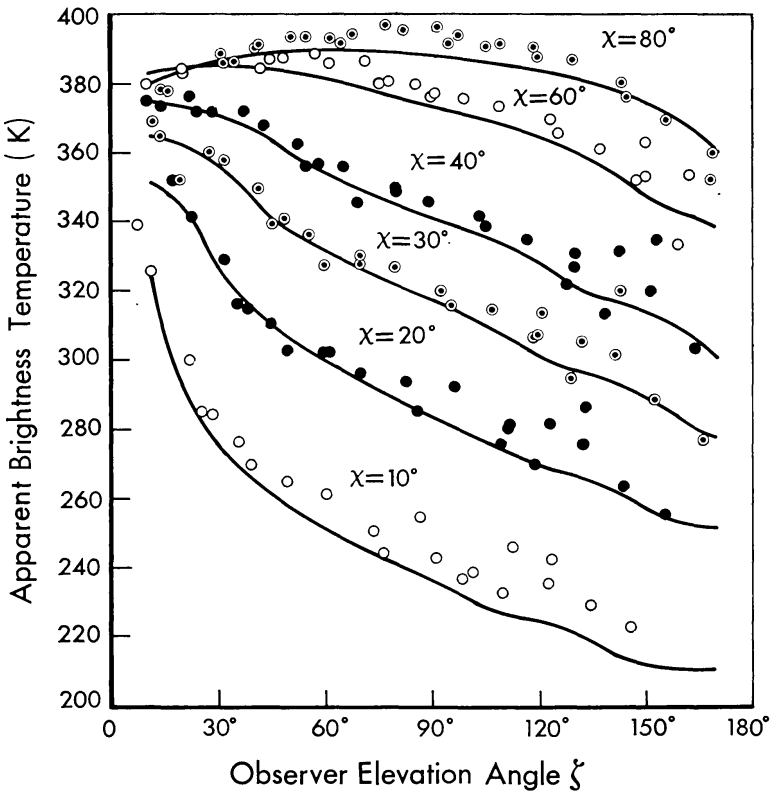

Fig. 8. Comparison of measured and calculated thermal meridian brightness temperatures.

Somewhat better agreement in certain ranges of ζ and χ can be achieved with greater areal fractions of subdued craters and fewer sharp ones. However, the crater geometry in the present model is too highly idealized to justify identification of an optimum distribution of crater configurations. In any case, it is fair to conclude from these results that the cratered soil model can reproduce most of the general features of the observed behavior of T_b as a function of ζ and χ.

The only significant disagreement between data and theory occurs at the highest sun angles, where the measured temperatures exceed those predicted by theory by 1 or 2%

* This conclusion differs quantitatively from that stated in an earlier discussion by Winter (1970). In the cited paper it was concluded that a relatively smaller fraction of sharply profiled craters could produce D-factor contour diagrams with an appearance similar to the observed pattern. However, the calculated D-factor diagram in that work has since been discovered to be incorrect, due to a programming error in the computation of apparent brightness temperature.

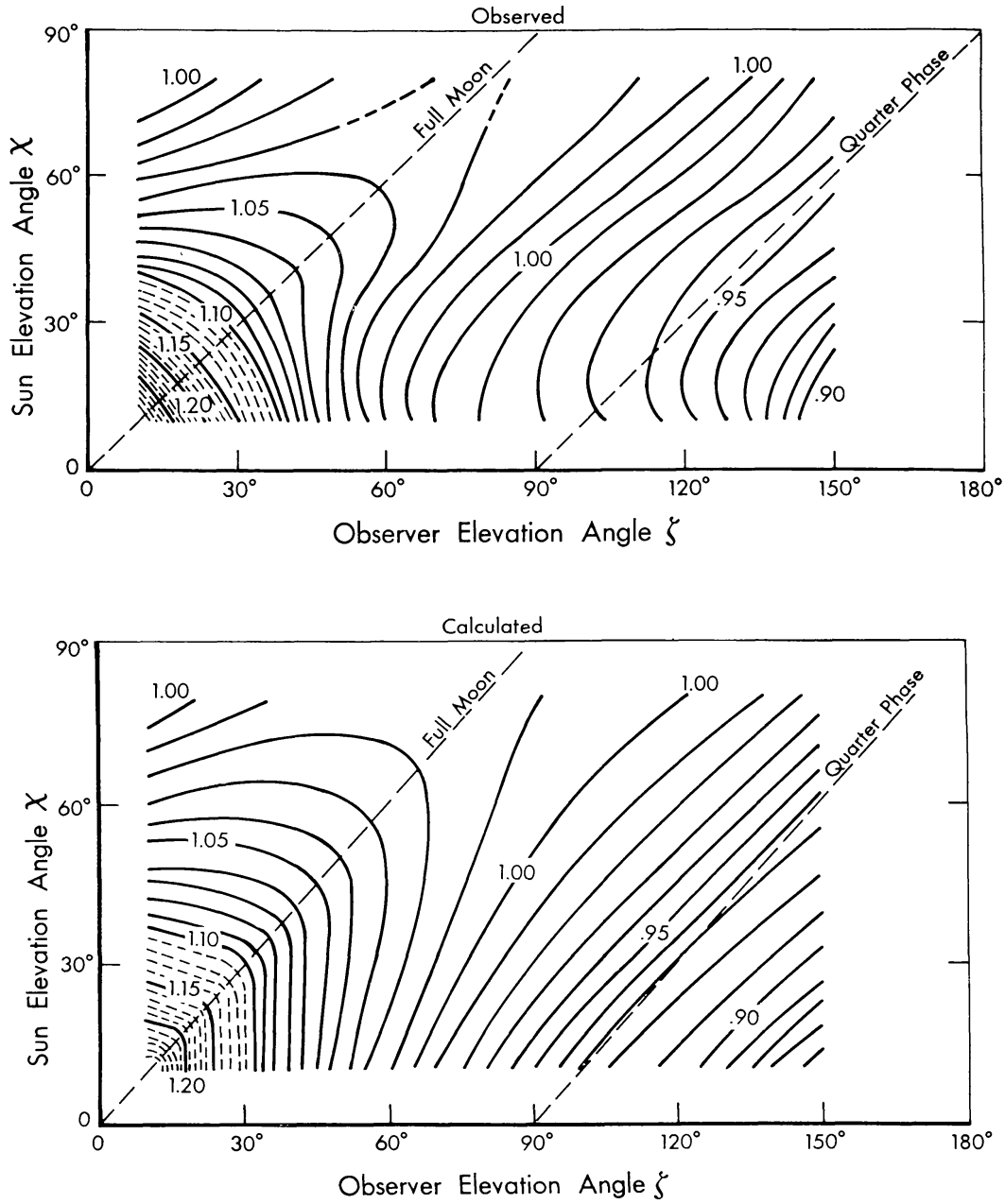

Fig. 9. Comparison of measured and calculated D-factor contours in the $\zeta - \chi$ plane.

over a range of observer angles about the zenith. Within the constraints of the model used in this study, it is not possible to account for the highest reported temperatures with craters of any realistic density and configuration. Furthermore, the difficulty cannot be resolved by adding surface rocks to the model since for ζ near 90° the brightness temperature would then tend to decrease slightly rather than exhibit the required enhancement.

At the present time, we can only indicate a few possible explanations for discrepancies at large values of χ. First, the possibility cannot be discounted that the reported measurements are too high because of errors in calibration at phase angles

around full-moon. Experimental uncertainties are compounded due to the fact that Saari and Shorthill used the subsolar point data reported by Sinton (1962) to calibrate their scans at each lunar phase. Thus, experimental errors in the surveys by the Boeing observers, when coupled with those in the subsolar point measurements at Lowell Observatory, may account for at least part of the disagreement at high sun angles.

It is equally probable that the discrepancy may be explained by inadequacies in the theoretical treatment. For example, it is a fact that a more realistic particulate soil model predicts a noontime overhead brightness temperature which is higher by the required amount (2%) than that predicted by the present continuum thermophysical model. In fact, a particulate model would give higher soil temperatures over a fairly wide range of observer angles as long as the Sun was within 30° of the zenith. Thus, the oversimplification of the thermal model appears as a likely candidate to account for the high sun angle discrepancy. Notwithstanding this explanation, an assessment of uncertainties in the reported measurements probably deserves equal priority with any attempt to refine the present theoretical treatment.

In summary, then, the present study demonstrates that infrared data from the lunar thermal meridian can be satisfactorily reproduced by calculations based on a simple model of a cratered lunar soil. Moreover, the crater population characteristics are consistent with observed intermediate-scale topography inasmuch as the inferred areal crater density is fairly high and the data is most satisfactorily reproduced by using representative crater configurations. It is therefore fair to conclude that surface roughness in the form of intermediate-scale craters is largely responsible for directional infrared emission characteristics of the Moon.

Acknowledgements

We are grateful to J. M. Saari and R. W. Shorthill for making available to us their original data and for several helpful discussions of this work.

References

Bastin, J. A. and Gough, D. O.: 1969, *Icarus* **11**, 289.
Buhl, D., Welch, W. J., and Rea, D. G.: 1968a, *J. Geophys. Res.* **73**, 5281.
Buhl, D., Welch, W. J., and Rea, D. G.: 1968b, *J. Geophys. Res.* **73**, 7593.
Gear, A. E. and Bastin, J. A.: 1962, *Nature* **196**, 1305.
Geoffrion, A., Korner, M., and Sinton, W. M.: 1960, *Lowell Obs. Bull.* **5**, 1.
Marcus, A.: 1966, *Icarus* **5**, 590.
Montgomery, C. G., Saari, J. M., Shorthill, R. W., and Six, N. F., Jr.: 1966, Boeing Document D1-82-0568, The Boeing Company, Seattle, Wash., U.S.A.
Morris, E. C. and Shoemaker, E. M.: 1968, 'Craters', Chapter III, Sec. G of *Surveyor Project Final Report*; Part II. Science Results, Tech. Rep. 32-1265, Jet Propulsion Laboratory, Pasadena, Calif.
Oberbeck, V. R. and Quaide, W. L.: 1967, *J. Geophys. Res.* **72**, 4697.
Pettit, E. and Nicholson, S. B.: 1930, *Astrophys. J.* **71**, 102.
Roelof, E. C.: 1968, *Icarus* **8**, 138.
Ross, H. P.: 1968, *J. Geophys. Res.* **73**, 1343.
Saari, J. M. and Shorthill, R. W.: 1967a, NASA Contractor Report NASA CR-855, prepared by the Boeing Scientific Research Laboratories, Seattle, Wash., U.S.A.

Saari, J. M. and Shorthill, R. W.: 1967b, 'Review of Lunar Infrared Observations', in *Physics of the Moon* (ed. by S. F. Singer), AAS, Science and Technology Series **13**, 57.
Sinton, W. M.: 1962, 'Temperatures on the Lunar Surface', Chapter 11 of the *Physics and Astronomy of the Moon* (ed. by Z. Kopal), Academic Press, New York and London.
Soderblom, L. A.: 1970, *J. Geophys. Res.* **75**, 2655.
Trask, N. J.: 1966, 'Size and Spatial Distribution of Craters Estimated from the Ranger Photographs', Ranger VIII and IX; Part II. Experimenters' Analyses and Interpretations, Tech. Rep. 32-800, Jet Propulsion Laboratory, Pasadena, California.
Trask, N. J.: 1967, *Icarus* **6**, 270.
Winter, D. F.: 1970, *Radio Science* **5**, 229.
Winter, D. F. and Saari, J. M.: 1969, *Astrophys. J.* **156**, 1135.